Second-order processes in heavy-ion collisions with application to ^{12}C-^{12}C reactions

Y. H. Chu, T. T. S. Kuo, and S. Y. Lee
Department of Physics, State University of New York at Stony Brook, Stony Brook, New York 11794
(Received 18 October 1983)

Semiclassical methods are used to analyze the second-order processes—the direct-one step process and the two-step process—in heavy ion collisions. Our main results are the following: (i) In the strong absorption limit, the direct one-step and two-step form factors are equally important and interfere destructively near the grazing angular momentum. The Austern-Blair theory gives satisfactory results for well-matched reactions. The angular distributions of mutual and double excitations are out of phase compared with that of the single excitation. (ii) For the weak to moderate absorption case, the internal part of the two-step process is enhanced. The angular distribution shows the refractive effect of overlapping resonances. Applications have been made to inelastic ^{12}C-^{12}C reactions.

I. INTRODUCTION

The second order processes in heavy-ion collisions provide an attractive and useful tool for the study of reaction mechanisms.[1-5] The Austern-Blair (AB) theory[6,7] has often been used to analyze this type of experimental data, but detailed understanding of such reaction processes is, however, still missing. It is known that the AB theory works very well in the strong absorption limit for the second-order processes,[6,7] but it is not yet known how to extend the AB theory to situations with weak to moderate absorption. In particular, how does the angular distribution change with decreasing absorption? The characteristics of the second-order processes, studied previously in the strong absorption limit, have been found to possess the following features:[8] (1) The angular distributions of double excitations oscillate out of phase with those of single excitations; (2) the envelope of the double excitation cross section decreases slowly with angle; and (3) there is strong destructive interference between the one-step and the two-step double excitation processes. Since semiclassical methods are useful in obtaining the detailed features[9-11] of the heavy-ion scattering, we shall apply them to the second-order process to find out some of the essential features mentioned above, and hopefully also understand the essential reaction mechanism in the weak to moderate absorption case. It should be pointed out, however, that our calculation is performed quantum mechanically, while the semiclassical method[9-11] is only used as a guide to our analysis.

The organization of our paper is as follows. In Sec. II, we shall study the form factor of the second-order processes in the strong absorption limit and then compare it to the AB theory. In Sec. III, we study the situation of weak absorption and examine the main effect of the overlapping molecular resonances in the radial integrals and in the angular distribution. The conclusions are given in Sec. IV.

We have used the optical potential from Ref. 9 for continuity. Although this potential does not fit the experimental data, general properties of these inelastic form factors derived in the present study represent those of all *deep* optical potentials.

II. SECOND-ORDER FORM FACTORS IN THE STRONG ABSORPTION LIMIT

In Appendix A, we review briefly the second-order inelastic form factor, which consists of a direct one-step (DOS) process,

$$B^{\mathrm{DOS}}_{l_f,l_i}(k_f,k_i)=\frac{\sqrt{4\pi}}{k_f k_i}\int f_{l_f}(k_f,r)V^{(2)}_T(r)f_{l_i}(k_i,r)dr\ , \tag{2.1}$$

and the two-step (TS) process,

$$B^{\mathrm{TS}}_{l_f,l_m,l_i}(k_f,k_m,k_i)=-\frac{2\mu\sqrt{4\pi}}{k_f k_m k_i}\int\int dr_1 dr_2 f_{l_f}(k_f,r_1)V^{(1)}_T(r_1)f_{l_m}(k_m,r_<)h^{(+)}_{l_m}(k_m,r_>)V^{(1)}_T(r_2)f_{l_i}(k_i,r_2)\ , \tag{2.2}$$

where f_l and $h^{(+)}_l$ are the regular and outgoing boundary condition distorted-wave functions, respectively. The radial transition potentials $V^{(2)}_T$ and $V^{(1)}_T$ are given in the collective model by

$$V^{(2)}_T(r)=\frac{\partial^2 V}{\partial R_0^2}\ , \tag{2.3}$$

$$V^{(1)}_T(r)=\frac{\partial V}{\partial R_0}\ , \tag{2.4}$$

R_0 being the nuclear radius. The exact second-order transition amplitude is given by Eq. (A12), and one observes that the second order inelastic form factor is given by

$$B_{l_f,l_m,l_i}(k_f,k_m,k_i)=B^{\rm DOS}_{l_f,l_i}(k_f,k_i)+2B^{\rm TS}_{l_f l_m l_i}(k_f,k_m,k_i)\ . \tag{2.5}$$

The relative phase of DOS and TS processes is important in the second-order form factor. To obtain some insight into inelastic form factors, we shall use the semiclassical decomposition of the distorted-wave (DW) functions into barrier and internal wave components (see the Appendix of Ref. 9).

Numerical application is carried out for the $^{12}C+^{12}C$ system at c.m. energy 30 MeV for the entrance channel using the optical potential shown in Table I. The second-order inelastic channels are the mutual excitation $^{12}C^*(4.44)+^{12}C^*(4.44)$, and the double excitation to a two phonon state $^{12}C^*(8.88\ \text{MeV})+^{12}C(0^+)$ with the process $^{12}C^*(4.44)+^{12}C(0^+)$ used as the intermediate channel. [Note that the $^{12}C^*(8.88\ \text{MeV},4^+)$ two phonon state does not exist in the realistic nuclear spectrum.]

TABLE I. The heavy ion nuclear optical potential is chosen to be

$$V(r)=-(V_0+iW_0)f(r-R,a_0,\alpha,a_1)\ ,$$

with

$$f^{-1}(S,a_0,\alpha,a_1)=1+\alpha e^{s/a_1}+e^{s/a_0}\ .$$

r_C is the Coulomb radius for the uniformly charged Coulomb potential.

V_0 (MeV)	W_0	r_0 (fm)	a_0 (fm)	α	a_1 (fm)	r_C (fm)
240	W_0	1.22	0.48	1.0	3.7	1.2

A. The DOS radial integral: $B^{\rm DOS}_{l_f l_i}(k_f,k_i)$

In the strong absorption limit, the DW f_l can be approximated by the barrier wave function f^B_l, which is a purely incoming wave inside the potential barrier, and so only the wave function in the barrier region will contribute to the barrier DOS radial integral, $B^{{\rm DOS}B}_{l_f l_i}$. Near the barrier, $V^{(2)}_T\cong(1/a)V^{(1)}_T$, where a is the diffuseness of nuclear potential, and so therefore,

$$B^{{\rm DOS}B}_{l_f,l_i}(k_f,k_i)=(1/\sqrt{4\pi}a)A^B_{l_f l_i}(k_f,k_i)\ , \tag{2.6}$$

where $A^B_{l_f l_i}$ is the barrier part of the radial integral defined in Ref. 9. This property of the DOSB term in Eq. (2.6) has been discussed extensively by Austern *et al.*[8]

B. TS radial integral $B^{\rm TS}_{l_f l_i}(k_f,k_i)$

1. *Properties of the function H*

The TS radial integral of Eq. (2.2) can be cast into the following form:

$$B^{\rm TS}_{l_f,l_m,l_i}(k_f,k_m,k_i)=-\frac{2\mu\sqrt{4\pi}}{k_m k_f k_i}\int dr(f_{l_f}V^{(1)}_T H_{l_m,l_i}f_{l_m}+f_{l_m}H_{l_m,l_f}V^{(1)}_T f_{l_i})\ , \tag{2.7}$$

where

$$H_{l_1 l_2}(k_1,k_2,r)=\int_r^\infty h^{(+)}_{l_1}(k_1,r')V^{(1)}_T(r')f_{l_2}(k_2,r')dr'\ . \tag{2.8}$$

Using the wave propagation matrix method of Ref. 11, $h^{(+)}_{l_1}(k_1,r)$ can be expressed as

$$h^{(+)}_{l_1}(k_1,r)\simeq i\sqrt{2k_1}\chi^{-1/4}_{l_1}e^{-i[S_{21}(l_1)+\delta_1(l_1)]}(-e^{-i[S_2(r)-\pi/4]}+N(l_1)e^{i[S_2(r)-(\pi/4)]})\ , \tag{2.9}$$

where $\sqrt{\chi_l}$ is the local wave number; S_{21}, δ_1, and $S_2(r)$ are semiclassical action integrals; and $N(l)$ is the barrier penetration factor (see Appendix B and Ref. 11). Thus, we have

$$\begin{aligned}H_{l_1 l_2}(k_1,k_2,r)\cong i\sqrt{k_1 k_2}e^{-i[S_{21}(l_1)+\delta_1(l_1)]}&\{N(l_1)N^{-1}(l_2)e^{i[S_{21}(l_2)+\delta_1(l_2)]}\\&+e^{-i[S_{21}(l_2)+\delta_1(l_2)]}[-N(l_2)-N(l_1)]\eta_I(l_2)\}I_0(l_1,l_2,r)\ ,\end{aligned} \tag{2.10}$$

with

$$I_0(l_1,l_2,r)=\int_r^\infty \chi^{-1/4}_{l_1}\chi^{-1/4}_{l_2}V^{(1)}_T(r)dr\ . \tag{2.11}$$

Since $N(l)\cong 1$, and $S_{21}(l)$ and $\delta_1(l)$ are slowly dependent on l,[10] we then have

$$H_{l_1 l_2}(k_1,k_2,r)=i\sqrt{k_1 k_2}e^{-\pi[\epsilon(l_2)-\epsilon(l_1)]+i[\delta_1(l_2)-\delta_1(l_1)]}(1-2e^{2\pi\epsilon(l_2)-2i\delta(l_2)})I_0(k_1,k_2,r)\ . \tag{2.12}$$

Equation (2.12) shows that weak absorption in the nuclear optical potential does not change the shape of the function $H_{l_1 l_2}$, whose magnitude in this case is only slightly modified for l_2 larger than the grazing angular momentum, where one has $\text{Re}[\epsilon(l_2)]>0$ (see Ref. 10). This shape of $H_{l_1 l_2}(k_1,k_2,r)$ is determined solely by $I_0(k_1,k_2,r)$. Since

$$[\chi_{l_1}(k_1,r)\chi_{l_2}(k_2,r)]^{-1/4}$$

depends slowly on r and

$$V^{(1)}_T=\frac{\partial V(r-R_0)}{\partial R_0}=-\frac{\partial}{\partial r}[V(r-R_0)]\ ,$$

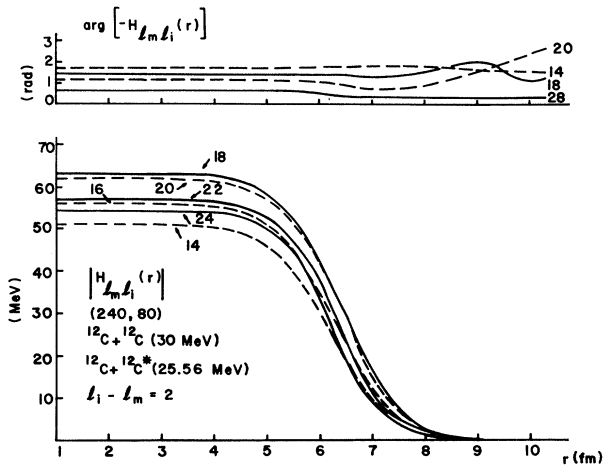

FIG. 1. The phases and amplitudes of $H_{l_m,l_i}(r)$ [Eq. (2.8)] are shown for $l_i - l_m = 2$. The depth of the optical potential is taken to be $(V_0, W_0) = (240,80)$ MeV.

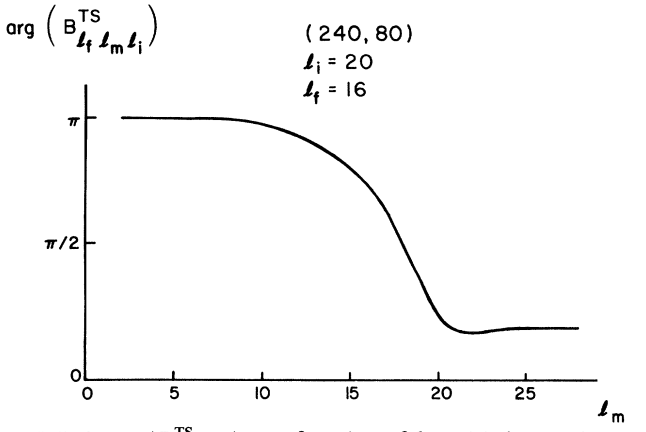

FIG. 2. $\arg(B^{TS}_{l_f,l_m,l_i})$ as a function of l_m, with $l_i = 20$, $l_f = 16$. It shows rapid change only at $l_m \simeq \Lambda_m$.

the integral (2.13) is proportional to $+V(r-R)$. However, for small l, $\arg(\chi_l^{-1/2}) \cong 0$ and for $l > L_{gr}$, $\arg(\chi_l^{-1/2}) \cong -\pi/2$, and so $\arg(-H_{l_1 l_2})$ decreases as the angular momentum increases. Figure 1 shows the amplitude and phase of $H_{l_m l_i}(k_m,k_i,r)$ for strong absorption and one notes that the function $H_{l_m l_i}(k_m,k_i,r)$ depends very little on the angular momentum l_m.

2. *Effective potential for the two-step process*

Through the definition of the function H, one can cast the radial integral of the TS process into the form of the direct one-step (DOS) process by defining the effective potential

$$V^{TS}_{eff} \equiv -\frac{2\mu}{k_m} V_T^{(1)}(r) \left[\frac{H_{l_m,l_i}(k_m,k_i,r)}{f_{l_i}(k_i,r)} + \frac{H_{l_m,l_f}(k_m,k_f,r)}{f_{k_f}(k_f,r)} \right] f_{l_m}(k_m,r) \, . \tag{2.13}$$

Thus the TS radial integral becomes

$$B^{TS}_{l_f,l_m,l_i} = \frac{\sqrt{4\pi}}{k_f k_i} \int f_{l_f}(k_f,r) V^{TS}_{eff}(r) f_{l_i}(k_i,r) dr \, . \tag{2.14}$$

Using Eq. (2.12), the effective potential in Eq. (2.13) can be written

$$V^{TS}_{eff}(r) \cong -2\mu i \chi_{l_m}^{-1/4} [\chi_{l_i}^{1/4} I_0(k_m,k_i,r) + \chi_{l_f}^{1/4} I_0(k_m,k_f,r)] V_T^{(0)}(r) \, . \tag{2.15}$$

We note some interesting properties of the $V^{TS}_{eff}(r)$:

(1) Since

$$I_0(k_1,k_2,r) \sim V_N(r) \to 0$$

(at large r), we expect that $V^{TS}_{eff}(r) \to 0$ (at large r) faster than $V_T^{(1)}(r)$. Thus, $V^{TS}_{eff}(r) \ll V_T^{(1)}(r)$ at the barrier region. This property will imply that $B^{TS}_{l_f,l_m,l_i}/B^{DOS}_{l_f,l_i} \to 0$ at large angular momentum, $l \gg \Lambda$.

(2) For fixed l_i and l_f, $V^{TS}_{eff}(r)$ depends on l_m through $\chi_m^{-1/4}(r)$. Thus the phase of $V^{TS}_{eff}(r)$ will drop from π to 0 at the grazing angular momentum (gam) Λ_m. Figure 2 shows that $\arg(B^{TS}_{l_f,l_m,l_i})$ (with $l_i = 20$, $l_f = 16$) varies rapidly as a function of l_m at $l_m \cong \Lambda_m$.

(3) The amplitude $|V^{TS}_{eff}(r)|$ peaks at $l_m \cong \Lambda_m$, thus $|B^{TS}_{l_f,l_m,l_i}|$ peaks at $l_m \cong \Lambda$.

Figure 3 shows $|B^{TS}_{l_f,l_m,l_i}|$ as a function l_m for given values of l_i and l_f. The dependence of $B^{TS}_{l_f,l_m,l_i}$ on l_m is smoother than its dependence on l_i and l_f. At first sight, this seems to indicate that an approximate method involving averaging over l_m would give good results. However, when the direct one-step B^{DOS} and two-step B^{TS} terms are combined together to form the total second order form factor B, they interfere destructively near the grazing angular momentum, as shown in the lower part of Fig. 3. This is due to the nonsmoothness of $\arg B^{TS}_{l_f,l_m,l_i}$ (see Fig. 2). Thus B_{l_f,l_m,l_i} varies rapidly with L_m near grazing angular momentum, and a detailed examination of this interference will now be given.

C. Interference between DOS and TS processes

The phases ϕ^{DOS} and ϕ^{TS} of $B^{DOS}_{l_f l_i}$ and $B^{TS}_{l_f,l_m,l_i}$ are shown in the lower part of Fig. 4. The behavior of these phases can be obtained in the following discussions:

(1) At large angular momentum, the phase of $H_{l_1 l_2}(r)$ is approximately zero (see Sec. II A), and so $V^{TS}_{eff}(r)$ has the same phase as $V_T^{(2)}(r)$ in the barrier region, where the local wave number is purely imaginary. Thus B^{DOS} and B^{TS} given in Eqs. (2.1) and (2.14) have the same phase.

(2) For small angular momentum, the distorted wave functions are almost purely incoming waves throughout the entire region of integration. If we define $F^{DOS}_{l_f,l_i}(r)$ and $F^{TR}_{l_f,l_m,l_i}(r)$ as

$$F^{DOS}_{l_f,l_i}(r) = \frac{\sqrt{4\pi}}{k_f k_i} \int_0^r f_{l_f}(k_f,r) V_T^{(2)} f_{l_i}(k_i,r) dr \, , \tag{2.16}$$

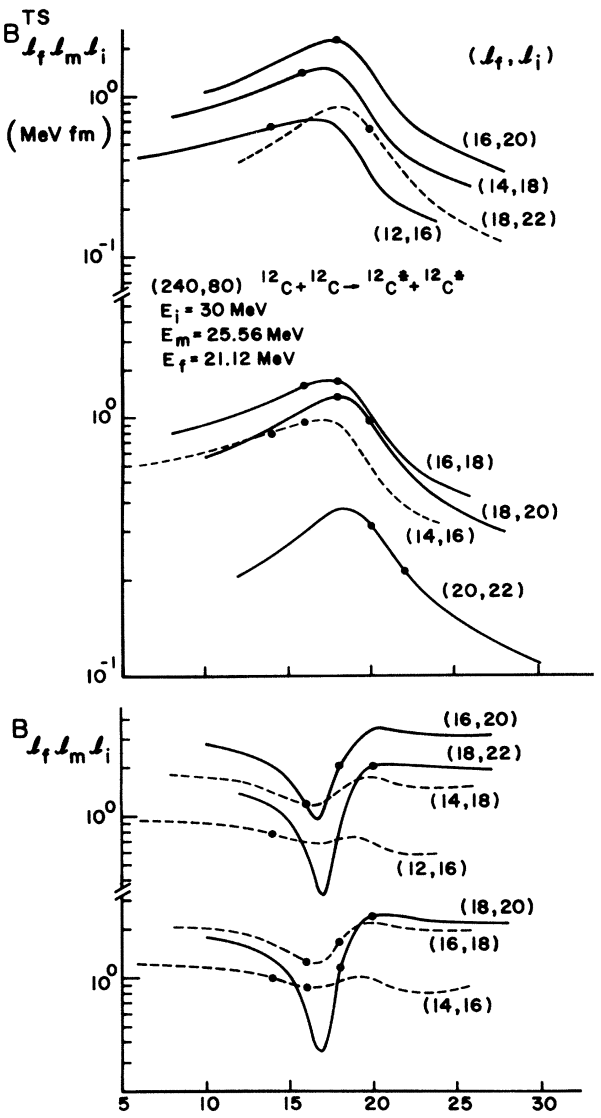

FIG. 3. Amplitudes of $B^{TS}_{l_f,l_m,l_i}$ and B_{l_f,l_m,l_i} [Eqs. (2.2) and (2.5)] as a function of l_m. The numbers in the bracket beside each curve are the corresponding (l_f,l_i). The dots on each curve indicate the allowed angular momentum of the intermediate channel for the reaction. Note that the destructive interference between DOS and TS processes gives rise to a rapidly varying function of l_m in the lower part of this figure.

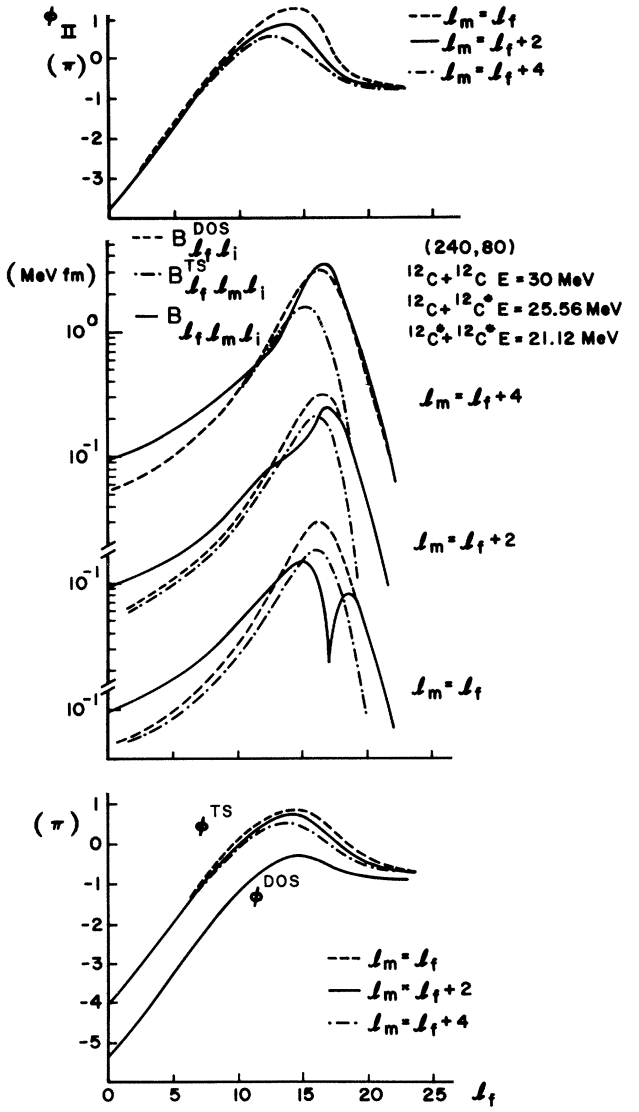

FIG. 4. The phases and amplitudes of $B^{DOS}_{l_f,l_i}$ and $B^{TS}_{l_f,l_m,l_i}$ are shown in the lower and middle parts of the figure. The phase and amplitude of the total second order radial integral B_{l_f,l_m,l_i} are shown in the upper and middle parts of the figure.

$$F^{TS}_{l_f,l_m,l_i}(r)=\frac{\sqrt{4\pi}}{k_f k_i}\int_0^r f_{l_f}(k_f,r)V^{TS}_{eff}(r)f_{l_i}(k_i,r)dr\ , \qquad (2.17)$$

we have then $B^{DOS}=F^{DOS}(r=\infty)$ and $B^{TS}=F^{TS}(r=\infty)$. The amplitudes and phases of Eqs. (2.16) and (2.17) are shown in Fig. 5, which indicates that the phase averaging[9,12] is very important. At small r, their arguments are proportional to $\arg(f_{l_f})+\arg(f_{l_i})$ with a constant phase difference

$$\arg(F^{TS})-\arg(F^{DOS})\simeq\pi/2\ .$$

However, the integration of F^{TS} is cut off earlier than F^{DOS} [$V^{TS}_{eff}(r)$ decreases faster in the tail region; see Sec. II B 2], so that the phase difference is increased by a value of order $\sim ka$ as $r\to\infty$. (Here k is the wave number, and a is the diffuseness of the nuclear potential, $ka\cong\pi/2$ in the present calculation). Thus, $\phi^{TS}-\phi^{DOS}\gtrsim\pi$ for small angular momentum.

(3) For l near the grazing angular momentum, the phase difference $\phi^{TS}-\phi^{DOS}$ changes from $\gtrsim\pi$ to zero. When the phase difference passes π, the DOS and TS terms interfere destructively. Figure 6 shows the interference effect of the DOS and TS processes near the grazing angular momentum.

D. Comparison with the Austern-Blair theory

Since the distorted wave function f_l satisfied the Schrödinger equation, the variation of f_l with respect to a change in the radius parameter R_0 of the optical potential can be expressed as

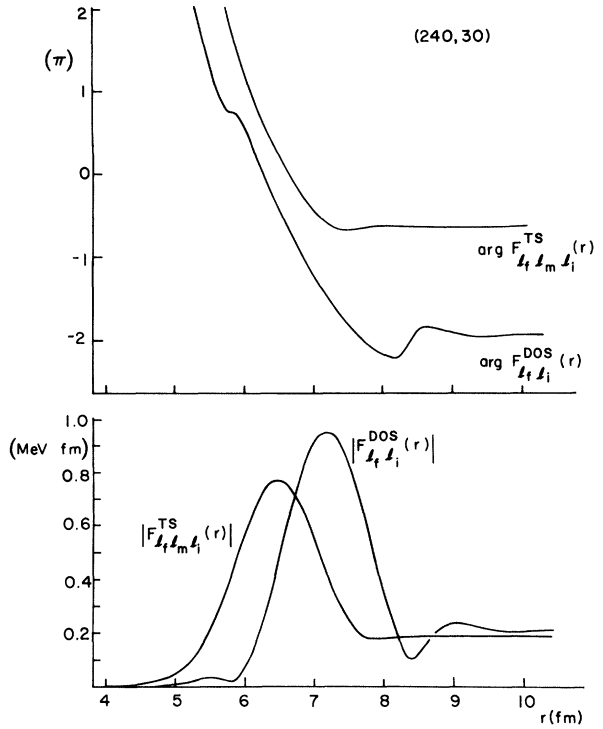

FIG. 5. The phase and amplitude of $F^{DOS}_{l_f l_i}(r)$ and $F^{TS}_{l_f l_m l_i}$ [Eqs. (2.16) and (2.17)] are shown to display the phase averaging effect of the radial integrals.

$$\frac{\partial f_l}{\partial R_0}=\frac{1}{E-T-V}\frac{\partial V}{\partial R_0}f_l$$
$$=-\frac{2\mu}{k}\int dr' f_l(r_<)h_l^{(+)}(r_>)\frac{\partial V}{\partial R_0}f_l(r')\ . \tag{2.18}$$

Hence, the variation of the first-order form factor $A_{l_f l_i}$ (see Ref. 9) with respect to R_0 gives us

$$\frac{\partial A_{l_f,l_i}}{\partial R_0}=\sqrt{4\pi}[B^{DOS}_{l_f,l_i}(k_f,k_i)$$
$$+B^{TS}_{l_f l_i l_i}(k_f,k_i,k_i)+B^{TS}_{l_f,l_f,l_i}(k_f,k_f,k_i)]\ . \tag{2.19}$$

The second order inelastic form factor in the AB theory is given by[6]

$$B^{AB}_{l_f,l_i}\equiv\tfrac{1}{2}[B_{l_f,l_f,l_i}(k_f,k_f,k_i)$$
$$+B_{l_f,l_i l_i}(k_f,k_i,k_i)]$$
$$=(1/\sqrt{4\pi})\frac{\partial}{\partial R_0}(A_{l_f l_i})\ . \tag{2.20}$$

Figure 6 compares the averaged second order radial integral with the derivative of the first order radial integral

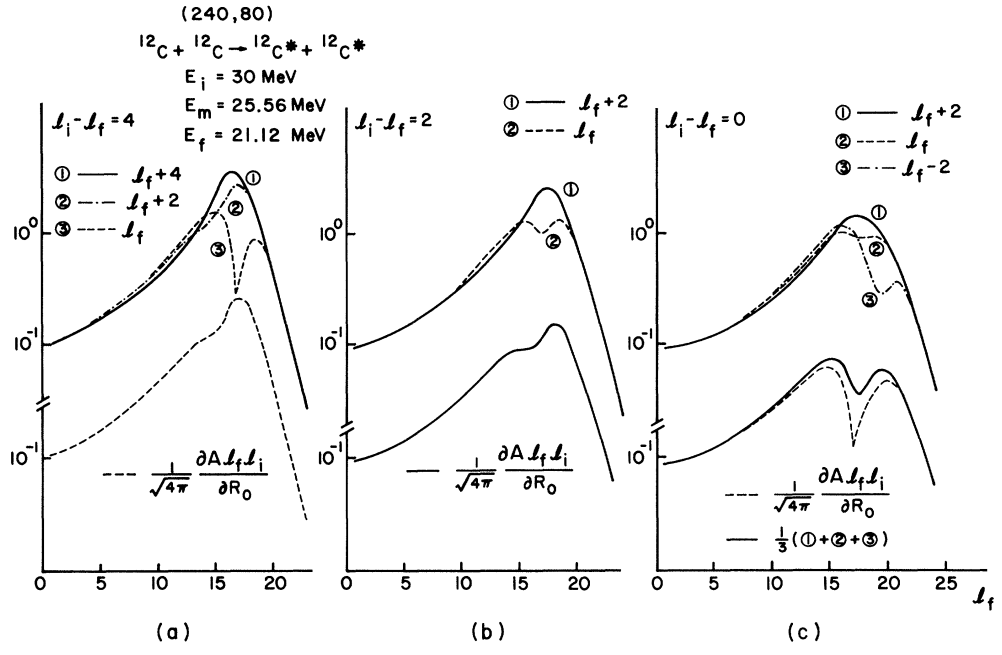

FIG. 6. (a) shows $B_{l_f l_m l_i}$ for $l_i-l_f=4$ with $l_m=l_f+4$, l_f+2, and l_f indicated as curves ①, ②, and ③, respectively. The lower dashed curve is the radial integral of the Austern-Blair theory, i.e.,

$$B^{AB}_{l_f l_i}=\frac{1}{\sqrt{4\pi}}\frac{\partial}{\partial R_0}A_{l_f l_i}\ ,$$

where $A_{l_f l_i}$ is the first order radial integral. Note here that the lower dashed curve (AB theory) matches exactly with the exact radial integral of curve ②. (b) shows $B_{l_f l_m l_i}$ for $l_i-l_f=2$. The lower solid curve is the AB radial integral. (c) shows $B_{l_f l_m l_i}$ for $l_i-l_f=0$. The lower solid curve is $B^{AB}_{l_f l_i}$, which is less accurate in comparison with curve 2. The lower dashed curve is $\frac{1}{3}$(①+②+③).

in Eq. (2.20). The reaction is

$$^{12}C+^{12}C\rightarrow ^{12}C+^{12}C^{*}(2^{+})\rightarrow ^{12}C^{*}(2^{+})+^{12}C^{*}(2^{+}) ,$$

i.e., the mutual excitation of two heavy ions, with $E_i=30$ MeV (c.m.). In this example, $\Lambda_i-\Lambda_m\simeq 2$, $\Lambda_m-\Lambda_f\simeq 2$, where Λ_i, Λ_m, and Λ_f are the gam of initial, middle, and final channels, respectively. Using the distorted wave property discussed in Ref. 8, i.e.,

$$f_{l_i}(k_i,r)\simeq f_{l_i-\xi}(k_m,r) ,$$

with $\xi\equiv\Lambda_i-\Lambda_m$, Eq. (2.20) becomes

$$B^{\mathrm{AB}}_{l_f,l_i}\cong\tfrac{1}{2}[B_{l_f,l_f+2,l_i}(k_f,k_m,k_i)+B_{l_f,l_i-2,l_i}(k_f,k_m,k_i)] . \tag{2.21}$$

For the reaction of the present calculation, we can have $|l_i-l_f|\leq 4$. Let us now consider the following three cases.

(a) $l_i-l_f=4$: The allowed value of l_m is l_f+2. Equation (2.21) is exact. Figure 6(a) shows that the dashed-dotted curve 2 with $l_m=l_f+2$ is identical to the lower curve with derivative approximation;

(b) $l_i=l_f+2$ and $l_m=l_f+2$ or l_f: The derivative approximation equals the averaged value of the exact second order radial integrals. Figure 6(b) shows that the lower curve is identical to the average of curves 1 and 2;

(c) $l_i=l_f$, $l_m=l_f+2$, l_f, or l_f-2: The corresponding radial integrals B_{l_f,l_m,l_f} are shown in Fig. 6(c) (curves 1, 2, and 3, respectively). In this case, the derivative procedure becomes less accurate, yet it retains the essential interference pattern near the grazing angular momentum. For $l_i=l_f-2$ and $l_i=l_f-4$, the Austern-Blair form factors become less accurate, but these form factors are relatively unimportant in the scattering process, and so we can conclude that the AB theory gives a fairly good approximation to the present calculation (see Refs. 6 and 7).

E. Angular distribution

The transition amplitude of inelastic excitations are listed in Appendix A for completeness (see Ref. 6). The second-order inelastic S matrix $S^{L}_{l_f l_i}$ is plotted as a function of l_f for $l_i-l_f=4,2,0$, etc., in Fig. 7, where the deformation length is taken to be 1 fm. $S^{L}_{l_f l_i}$ closely resembles the radial integrals for $L=0$, 2, and 4 discussed in Secs. II B–D, while only the TS process contributes to the $L=1,3$ terms. Because of the kinematic matching condition, $S^{4}_{l_f,l_f+4}$ is larger than the other inelastic S-matrix elements. The angular distribution curves are shown in Fig. 8 for $L=0$, 1, 2, 3, and 4, respectively, where the $L=4$ component dominates because of the kinematic matching condition and, more importantly, its larger statistical weight. Other L components have the important effect of reducing the peak-to-valley ratio of the diffraction pattern

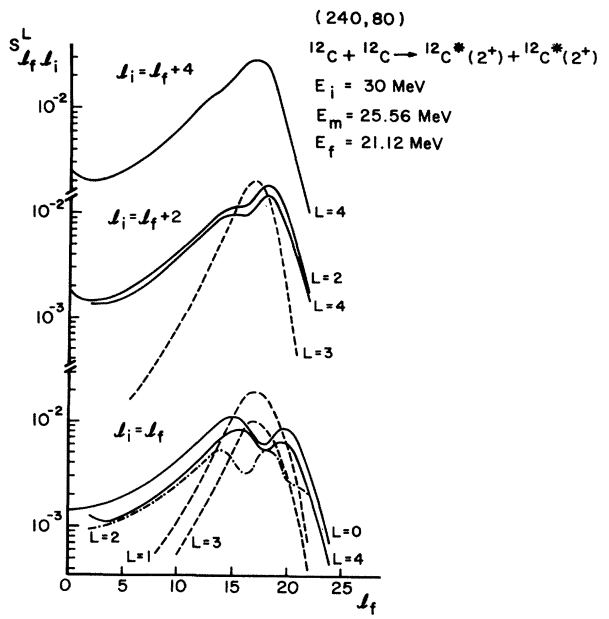

FIG. 7. Inelastic S matrix $S^{L}_{l_f l_i}$ [Eq. (A13)] are shown for $l_i-l_f=4$, 2, and 0, respectively.

in the angular distribution. Note also that the angular distributions of even L are out of phase with that of odd L (see the discussion of Sec. II F).

On the upper part of Fig. 8, we plot the angular distribution of the inelastic excitation to a single excitation of $^{12}C(4^{+})$ at 8.88 MeV. The corresponding $^{12}C(4^{+})$ double exciton cross section is given by the curve marked by $L=4$ and the mutual excitation cross section is marked by the mutual. We observe that the diffraction pattern looks the same as that of the one-step inelastic excitation, but note that the slope of angular distribution in the case of mutual excitation is much smaller than that for single excitation. This is due to the fact that interference of TS and DOS processes are important in the mutual excitations (see Fig. 7 and Ref. 8).

Figure 9 decomposes the angular distribution into DOS and TS components, where we see that the DOS and TS components interfere destructively at grazing (forward) angles and the angular distribution is dominated by the TS processes at larger angles. This is a general property of the angular distribution of the second-order processes. Most of these properties have previously been demonstrated in the strong absorption limit.[8]

F. Poisson sum formula and analytic expression of the scattering amplitude

Using the Poisson sum formula (see Ref. 13), one obtains the single excitation scattering amplitude F^{M}_{L}

$$F^{M}_{L}=[L:M]\frac{L+\frac{1}{2}}{\pi(2\sin\theta)^{1/2}}\frac{\sqrt{(L-M)!(L+M+1)!}}{\Gamma(L+\frac{1}{2})}e^{(1/2)i[M-(1/2)]\pi}$$

$$\times\sum_{m=-\infty}^{\infty}(-)^{m}\tfrac{1}{2}[F^{(-)}_{m}(\theta)-ie^{-iM\pi}F^{(+)}_{m}(\theta)+e^{-iM\pi}F^{(-)}_{m}(\pi-\theta)-iF^{(+)}_{m}(\pi-\theta)] , \tag{2.22}$$

for identical ions with

$$F_m^{(\mp)}(\theta)=\int_{-\infty}^{\infty} d\lambda\, e^{i(2\sigma_{\lambda-(1/2)}+2m\lambda\pi\mp\lambda\theta)} i\frac{\sqrt{\pi}E}{k^2}\frac{\partial\eta_\beta}{\partial\Lambda}$$
$$\cong -i\frac{\sqrt{\pi}E}{4k^2}e^{i[2\sigma_\Lambda+\Lambda(2m\pi\mp\theta)]+\gamma\Delta(2m\pi+\Theta_C\mp\theta)}\left[\frac{\pi\Delta\,|\,2m\pi+\Theta_C\mp\theta\,|}{\sinh(\pi\Delta\,|\,2m\pi+\Theta_C\mp\theta\,|\,)}\right], \tag{2.23}$$

where the Ericson parametrization for η_β has been used in arriving at Eq. (2.23). θ_C is the Coulomb deflection angle evaluated at the grazing angular momentum Λ. $[L:M]$ is given by Ref. 6, i.e.,

$$[L:M]=\sum_x i^x\langle l_f 0L\,0\,|\,l_f+x,0\rangle\langle l_f-M,LM\,|\,l_f+x,0\rangle$$
$$=\begin{cases} i^L\dfrac{\sqrt{(L-M)!(L+M)!}}{(L-M)!!(L+M)!!} & L+M=\text{even} \\ 0 & L+M=\text{odd}\,, \end{cases} \tag{2.24}$$

and we further make the following approximation:

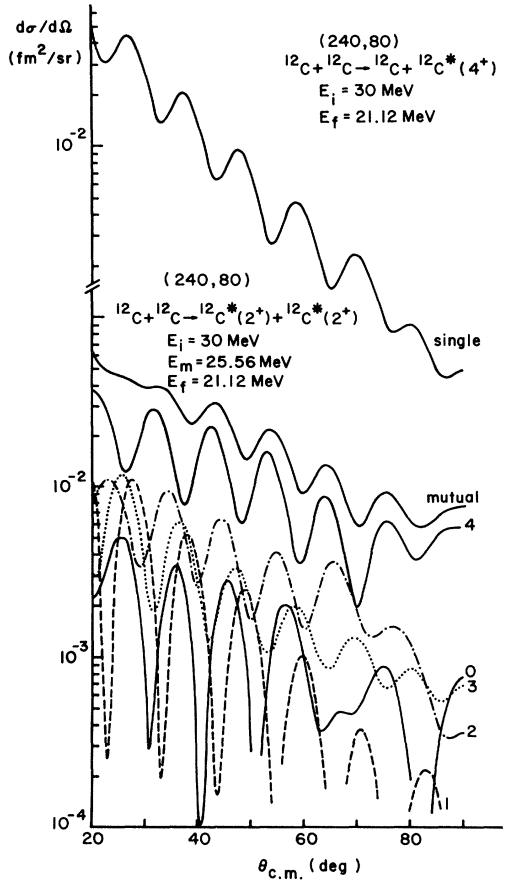

FIG. 8. Angular distribution of one-step DWBA $^{12}C(4^+,8.88$ MeV) excitation (upper curve) is compared with those of mutual, $^{12}C(2^+)+^{12}C(2^+)$, and double, $^{12}C[(2^+\times 2^+)4^+,8.88$ MeV] excitations, which is the $L=4$ component of the mutual cross section. Numbers beside these lower curves are the corresponding angular momentum transfer of the mutual excitation.

$$\sum_x i^x\langle l_f 0L\,0\,|\,l_f+x,0\rangle\langle l_f-M,LM\,|\,l_f+x,0\rangle A_{l_f,l_f+x}$$
$$\cong[L:M]\frac{i\sqrt{\pi}E}{k_f^2}\left[\frac{\partial\eta_\beta}{\partial\Lambda}\right]. \tag{2.25}$$

Equation (2.24) gives a selection rule to the allowed M value for a given L. For a given L value, $|F_L^M|^2$ will be in phase for each allowed M values, providing that Eq. (2.5) is valid. With the approximation of Eq. (2.25), the diffraction pattern of $\sum_M |F_L^M|^2$ for even and odd L values are out of phase with each other.

The important Poisson terms for $0<\theta\ll\pi/2$ are $F_0^-(\theta)$ and $F_0^+(\theta)$, while $F_0^-(\pi-\theta)$ and $F_0^+(\pi-\theta)$ dominate in the region $\pi/2\ll\theta<\pi$. These four terms interfere at $\theta\cong\pi/2$. We consider only the case $0<\theta\ll\pi/2$. The scattering amplitude becomes

$$F_L^M\propto[F_0^-(\theta)-ie^{iM\pi}F_0^+(\theta)]\,, \tag{2.26}$$

and the second order scattering amplitude in the AB theory is then given by

$$\frac{dF_L^M}{dR_0}\simeq k\frac{dF_L^M}{d\Lambda}\propto -ik\theta[F_0^-(\theta)+ie^{iM\pi}F_0^+(\theta)]\,. \tag{2.27}$$

The maximum of $|F_L^M|^2$ occurs at $\theta=\theta_1$, where

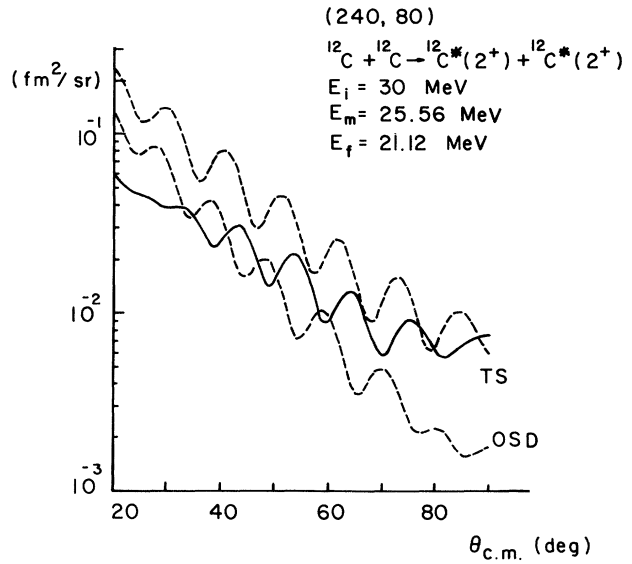

FIG. 9. Decomposition of the mutual cross section into two-step (TS) and direct one-step (OSD in this figure) components. The destructive interference of TS and DOS components at the grazing angle is the important feature of the angular distribution.

$$2\Lambda\theta_1=(2n-M-\tfrac{1}{2})\pi\ , \tag{2.28a}$$

while the maximum of $|dF_L^M/dR_0|^2$ occurs at θ_2, where

$$2\Lambda\theta_2=(2n-M+\tfrac{1}{2})\pi\ . \tag{2.28b}$$

Thus the angular distribution of the mutual (or double) excitation will be out of phase compared with that of the single excitation (Ref. 6). These properties are shown explicitly in Figs. 7 and 8. Since the dominant contribution of the mutual excitation comes from the $L=4$ components, the angular distributions of mutual and double excitation are thus expected to be in phase with each other (see Fig. 7).

From Fig. 9, we also observe that the DOS angular distribution is out of phase with that of the second-order angular distribution (solid line), i.e., the DOS angular distribution is *in* phase with the angular distribution of the single excitation. This is expected, because $B_{l_f l_i}^{\rm DOS}\sim(1/a)A_{l_f l_i}$ [see Eq. (2.6) and Ref. 8].

III. EFFECT OF THE UNDAMPED OVERLAPPING RESONANCES

When the imaginary potential becomes smaller, potential resonances will become important in the scattering process. At first, these resonances will work collectively to give rise to a semiclassical deflection function (see Appendix C). As the imaginary potential decreases further, each single resonance will become important in the scattering process, but in the heavy-ion collision, the latter situation may not be realized because of the large number of open channels.

A. DOS process

As shown in Ref. 9, we may write the distorted wave function as

$$f_l(k,r)=f_l^B(k,r)+f_l^I(k,r)\ .$$

One can decompose the radial integral into the barrier component of Sec. II A and the internal component $B_{l_f l_i}^{\rm DOSI}$ where

$$\begin{aligned}B_{l_f,l_i}^{\rm DOSI}&\simeq\frac{\sqrt{4\pi}}{k_f k_i}\int dr[f_{l_f}^I(k_f,r)V_T^{(2)}f_{l_i}^B(k_i,r)\\&\qquad+f_{l_f}^B(k_f,r)V_T^{(2)}f_{l_i}^I(k_i,r)]\\&\simeq\frac{2\pi}{k_f k_i}(\eta_I^f+\eta_I^i)\int dr\,V_T^{(2)}\\&\simeq 0\ ,\end{aligned} \tag{3.1}$$

with $V_T^{(2)}$ given by Eq. (2.3). Here η_I^f and η_I^i are the internal S matrices of the final and initial channels, respectively, and one obtains

$$B_{l_f,l_i}^{\rm DOS}(k_f,k_i)\simeq B_{l_f,l_i}^{{\rm DOS}B}(k_f,k_i)\ . \tag{3.2}$$

The dashed lines of Fig. 10 show the DOS component of the radial integral at weak absorption. (The DOS radial integral at $W_0=30$ MeV is indistinguishable from that of $W_0=80$ MeV.)

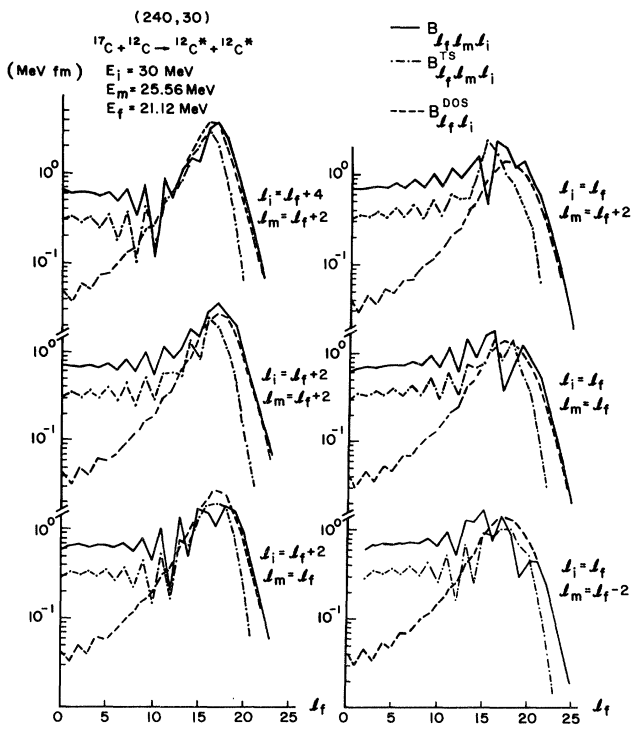

FIG. 10. Effect of undamped overlapping resonances are shown to be important for the TS radial integral but not important for the DOS radial integrals.

B. The internal wave component of the TS process

The effect of the internal wave component will modify not only the initial and final DW functions, but also the effective transition potential of Eq. (2.13). We shall examine the H function of Eq. (2.8) and the internal part of the radial integral.

1. The H function

Since $f_l(k,r)=f_l^B(k,r)+f_l^I(k,r)$ the $H_{l_1 l_2}(r)$ defined in Eq. (2.8) can be expressed as

$$H_{l_1 l_2}(r)=(1-2e^{2iS_{32}(l_2)})H_{l_1 l_2}^B(r)\ , \tag{3.3}$$

where $H_{l_1 l_2}^B(r)$ is the H function of strong absorption in Eq. (2.12) and we have used the stationary phase approximation to obtain Eq. (3.3). At resonance angular momentum l_2, i.e.,

$$\mathrm{Re}[S_{32}(l_2)]=[n+(1/2)]\pi\ ,$$

$H_{l_1 l_2}(r)$ will be enhanced. Figure 11 shows $|H_{l_m l_i}(r=0)|$ as a function $l_m=l_i-2$ with different imaginary potential strengths W_0. However, these pronounced oscillations ap-

pear for angular momenta far above the grazing angular momentum and their effect will not be very important in the scattering process (even at $W_0=10$ MeV). Similar conclusions can also be drawn for the effective potential.

2. The internal TS radial integral $B^{TSI}_{l_f,l_m,l_i}$

Decomposing the wave functions into barrier and internal parts, one gets

$$B^{TS}_{l_f,l_m,l_i}=B^{TSB}_{l_f,l_m,l_i}-\frac{4\mu\sqrt{\pi}}{k_m k_f k_i}\left[\int dr(f^B_{l_f}V^{(1)}_T H_{l_m l_i} f^I_{l_m}+f^I_{l_f}V^{(1)}_T H_{l_m l_i} f^B_{l_m})+(l_i\leftrightarrow l_f)\right], \tag{3.4}$$

where the properties of $B^{TSB}_{l_f l_m l_i}$, the barrier term, have been discussed in Secs. II B and II C and where the second-order contributions to the internal part of the elastic S matrix η_I have been neglected. Using the stationary phase approximation in the radial integral, we obtain

$$\begin{aligned}B^{TS}_{l_f,l_m,l_i}&\cong B^{TSB}_{l_f,l_m,l_i}+c_1\eta^f_I+c_2\eta^m_I+c_3\eta^i_I\\&\equiv B^{TSB}_{l_f,l_m,l_i}+B^{TSI}_{l_f,l_m,l_i},\end{aligned} \tag{3.5}$$

with

$$\begin{aligned}c_1&\simeq -i2\mu/\sqrt{k_f k_i}\,e^{-i[S_{21}(l_f)+\delta_1(l_f)-S_{21}(l_i)-\delta_1(l_i)]}X(l_f,l_m,l_i),\\c_3&\simeq c_1(l_i\leftrightarrow l_f),\\c_2&\simeq -i2\mu/\sqrt{k_f k_i}\,e^{i[S_{21}(l_f)+\delta_1(l_f)+S_{21}(l_i)+\delta_1(l_i)-2S_{21}(l_m)-2\delta_1(l_m)]}[X(l_f,l_m,l_i)+X(l_i,l_m,l_f)],\end{aligned}$$

where

$$X(l_f,l_m,l_i)=\int_0^\infty \chi^{-1/4}_{l_f}\chi^{-1/4}_{l_m}V^{(1)}_T(r)I_0(l_m,l_i,r)dr$$

and $I_0(l_1,l_2,r)$ is given by Eq. (2.11). Although η_I may be small, the coefficients c_1, c_2, and c_3 are given by radial integrals of $[V^{(1)}_T(r)]^2$, which is very large, and so the radial integrals for the second order processes are much more sensitive to the absorption than those for the first-order process. At $W_0=40$ MeV, the radial integral $A_{f_1 l_i}$ for the first-order process has already reached the strong absorption limit, while the radial integrals $B^{TS}_{l_f,l_m,l_i}$ for the second-order process require a much larger imaginary potential ($W_0=80$ MeV) to reach the same limit. Figure 10 shows the magnitude of $B^{TS}_{l_f,l_m,l_i}$ (dashed-dotted line) and

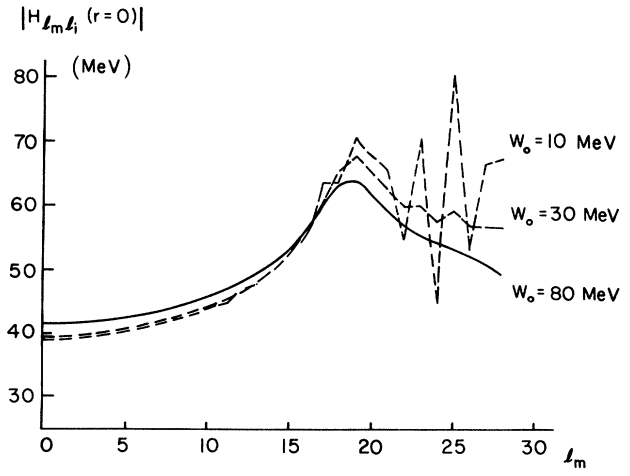

FIG. 11. Effect of the overlapping resonances is shown in this figure for the H functions. We note that the H functions are not very sensitive to the strength, W_0, of the imaginary potential. These overlapping resonances affect mainly the distorted wave functions in the two-step radial integrals [see Eq. (3.4)].

$$B_{l_f,l_m,l_i}=B^{DOS}_{l_f l_i}+2B^{TS}_{l_f,l_m,l_i}$$

(solid) at $W_0=30$ MeV. One observes that the potential resonances are much more important in second-order than first-order processes (see Ref. 9 for comparison). A few observations can be noted at this point:

(1) At low angular momentum,

$$2\,|B^{TS}_{l_f,l_m,l_i}|\gg|B^{DOS}_{l_f l_i}|,$$

and so

$$|B_{l_f,l_m,l_i}|\cong 2\,|B^{TS}_{l_f,l_m,l_i}|.$$

The oscillatory structure in these radial integrals comes from the interference between the $B^{TSB}_{l_f,l_m,l_i}$ and $B^{TSI}_{l_f,l_m,l_i}$, i.e., the two-step process.

(2) At larger angular momentum, $|B^{DOS}|\gg 2|B^{TS}|$ for moderate absorption.

(3) Around the grazing angular momentum, the interference between TS and DOS processes is important. At the grazing angular momentum this destructive interference (see Sec. II C) will give rise to a smaller slope in the angular distribution in comparison to that of the double excitation or single excitation. Figure 12 clearly shows this effect (see Figs. 8 and 9 for comparison).

C. Weak absorption situations

When the absorptive potential becomes weaker, the internal wave S matrix will become larger. At $W_0=10$ MeV, Fig. 13 shows semiclassical action integrals and elastic S matrices of entrance middle and final channels. We observe that $|\eta_I|\cong 0.2$, which is a little bit too large when compared with the S matrix which fits the $^{12}C+^{12}C$ elastic data ($|\eta_I|\simeq 0.15$ at 30 MeV, Ref. 14). It is worth pointing out that there is no multiple reflection in the potential pocket even at $W_0=10$ MeV (all resonances over-

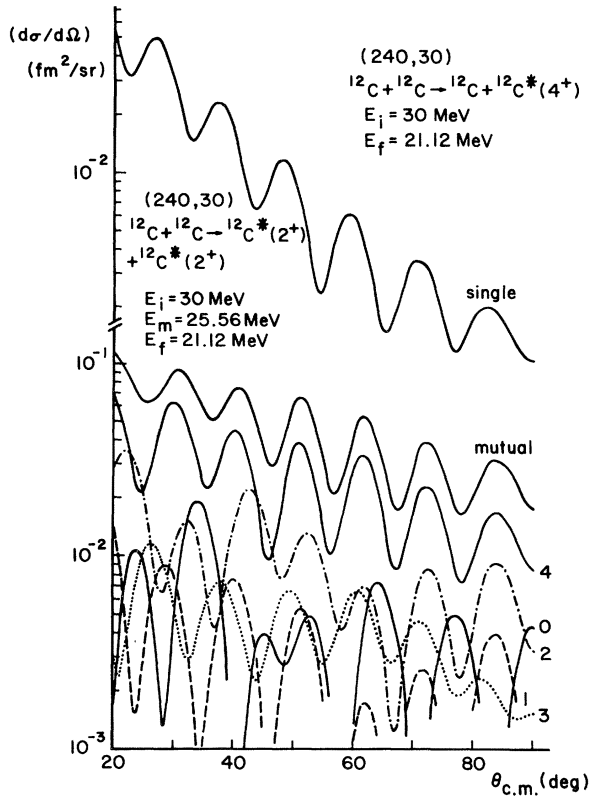

FIG. 12. Angular distribution for $W_0=30$ MeV. See the caption of Fig. 8 for comparison.

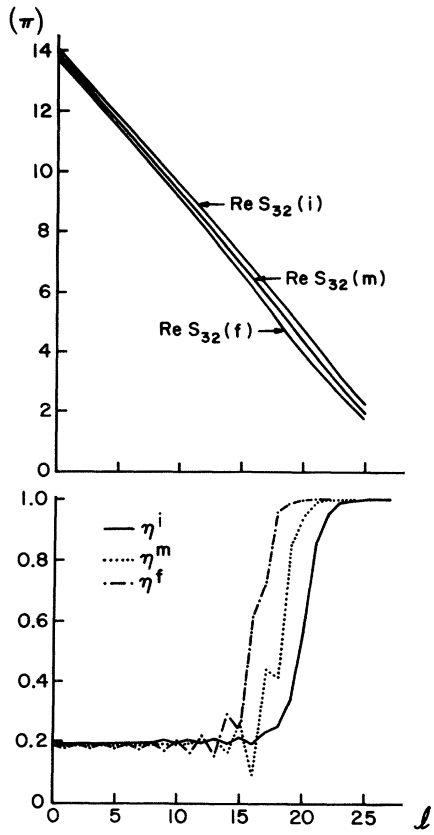

FIG. 13. Classical action integrals between the potential pockets of initial, middle, and final channels are shown in the upper part of the figure. The corresponding semiclassical elastic S matrices are shown in the lower part for $W_0=10$ MeV.

lap to a high degree).

With $W_0=10$ MeV, the TS radial integral is the dominant component of the second order form factor. Figure 14 shows that

$$B_{l_f,l_m,l_i}\cong 2B^{\mathrm{TS}}_{l_f,l_m,l_i}\ .$$

The interference between the $B^{\mathrm{TS}B}_{l_f l_m l_i}$ and $B^{\mathrm{TS}I}_{l_f l_m l_i}$ is also small and localized only near grazing angular momentum, and the $B^{\mathrm{DOS}}_{l_f,l_i}$ plays a little role in the scattering process. Figure 15 shows the amplitudes of the inelastic S matrices [Eq. (A13)]; one would then expect that the refractive effect is the major scattering process.

To study the characteristics of the angular distribution in the weak absorption limit, we first note that

$$B^{\mathrm{TS}}_{l_f l_m l_i}\cong B^{\mathrm{TS}I}_{l_f l_m l_i}$$

$$\cong c_1\eta^f_i(l_f)+c_2\eta^m_I(l_m)+c_3\eta^i_I(l_i)$$

[Eq. (3.5)]. If only even l_m contribute (identical ions) we can replace $B^{\mathrm{TS}I}_{l_f,l_m,l_i}$ by its average value, $\bar{B}^{\mathrm{TS}I}_{l_f,l_i}$, because $\eta^m_I(l_m)\cong\eta^{i,f}_I(l_m\pm 2)$ for $l_m<\Lambda_m$, the grazing angular momentum of the middle channel. Equation (A13) gives us then the inelastic S matrix

$$S^L_{l_f,l_i}\simeq i\frac{\mu k_i k_f}{2\pi^{3/2}}\delta_{l_1}\delta_{l_2}\langle l_f,0,L,0\,|\,l_i,0\rangle\langle l_1 0,l_2 0\,|\,L\,0\rangle i^{l_i-l_f}\bar{B}^{\mathrm{TS}I}_{l_f,l_i}\ . \tag{3.6}$$

Figure 15 indeed shows that the magnitude of even L components are much larger than that of odd L components. [Equation (3.6) neglects all the odd L components.] Since $\bar{B}^{\mathrm{TS}I}_{l_f,l_i}\sim\bar{c}_1\eta_I(l_f)+\bar{c}_2\eta_I(l_i)\approx c\eta_I(l_f)$, one can then obtain

$$\sum_x i^x\langle l_f,0L\,0\,|\,l_f+x,0\rangle\langle l_f-M,L,M\,|\,l_f+x,0\rangle c\eta_I(l_f)\simeq[L:M]ce^{2i\varphi(l_f)}\,|\,\eta_I(l_f=0)|\ , \tag{3.7}$$

where $[L:M]$ is defined in Eq. (2.24). Thus the scattering amplitude F^M_L is given by the following Poisson sum formula

$$F^M_L(\theta)=[L:M]\frac{e^{-i/2[M-(1/2)]\pi}}{2\pi(2\sin\theta)^{1/2}}\sum_{m=-\infty}^{\infty}(-)^m[I^{(-)}_m(\theta)+ie^{iM\pi}I^{(+)}_m(\theta)+e^{-iM\pi}I^{(-)}(\pi-\theta)-iI^{(+)}_m(\pi-\theta)]\ , \tag{3.8}$$

with

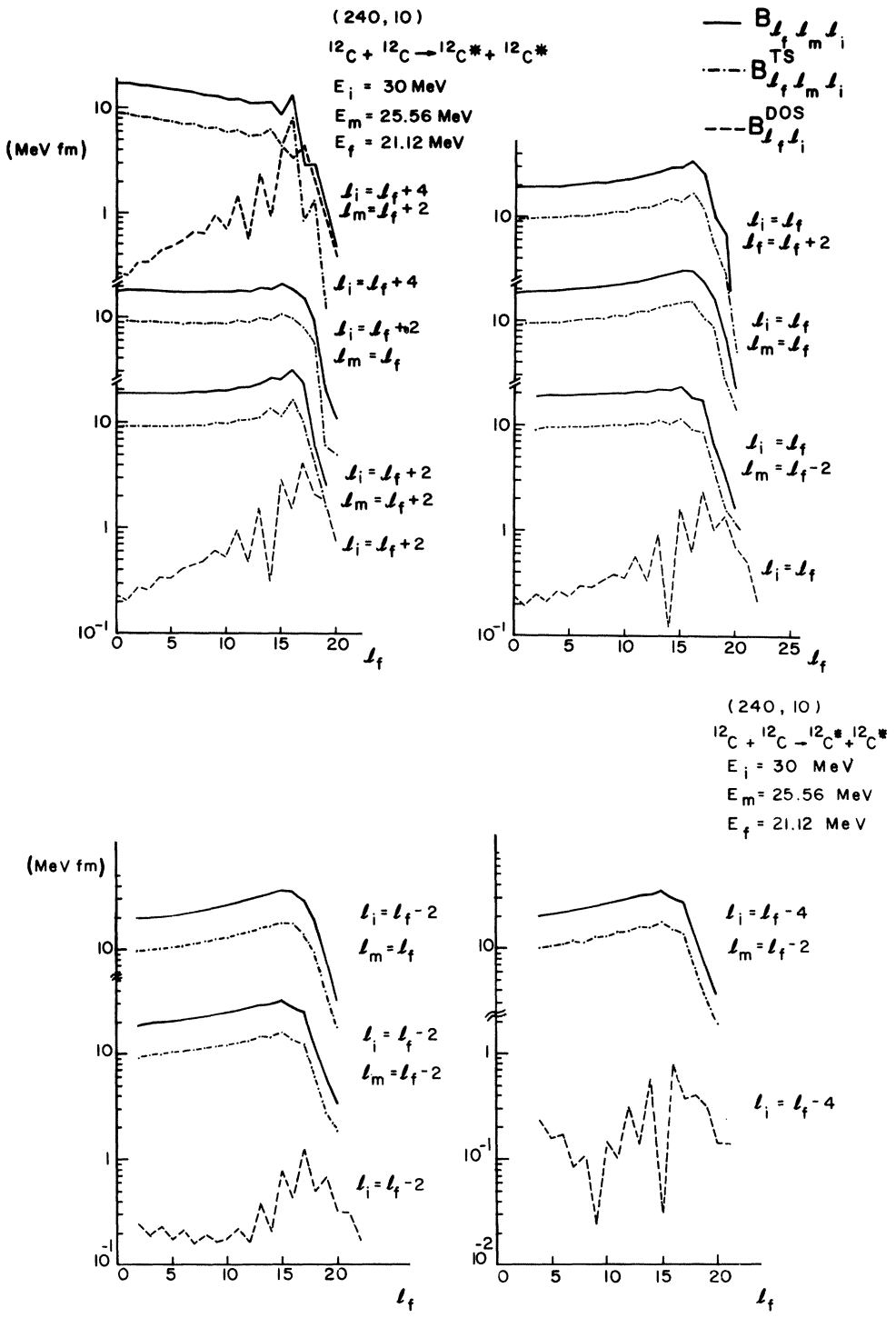

FIG. 14. The second order form factor B_{l_f,l_m,l_i} is about $B^{TS}_{l_f,l_m,l_i}$ in the weak absorptive case ($W_0 = 10$ MeV). The dashed line on this figure shows the contribution due to the DOS process.

$$I_m^{(\pm)}(\theta) = c \mid \eta_I(0) \mid \int_{-\infty}^{\infty} d\lambda \frac{[(\lambda - M - \frac{1}{2})!(\lambda + M + \frac{1}{2})!]^{1/2}}{\Gamma(\lambda+1)} \lambda e^{i[2\sigma_{\lambda-(1/2)} + 2m\pi\lambda \mp \lambda\theta + 2\varphi(\lambda)]} . \tag{3.9}$$

The main contribution to the above integral is expected to come from the point of stationary phase. Defining the deflection angle ($\lambda = l + \frac{1}{2}$),

$$\Theta(\lambda) \equiv \frac{d}{d\lambda}[2\varphi(\lambda) + 2\sigma_{\lambda-(1/2)}] = \Theta_N(\lambda) + \Theta_C(\lambda) , \tag{3.10}$$

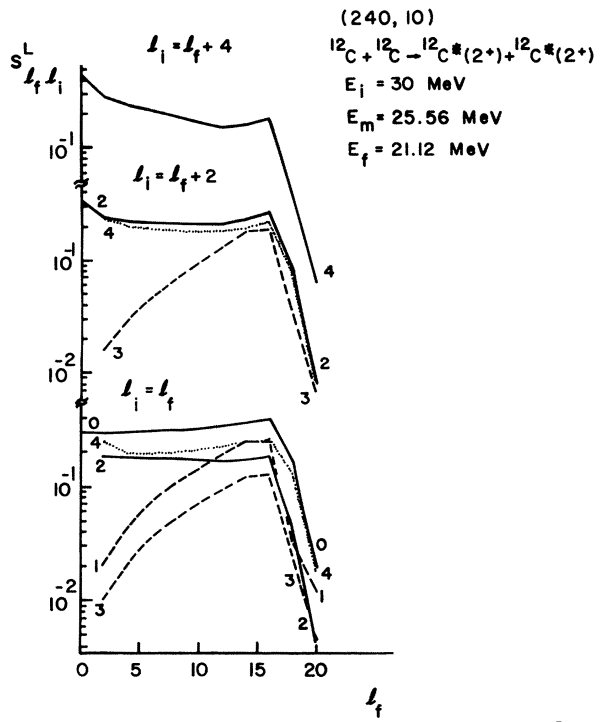

FIG. 15. The amplitudes of the inelastic S matrices $S^L_{l_f,l_i}$ are shown in this figure. Since the amplitudes are smooth functions of l_f, we expect that the refractive effect may be important (see Fig. 16).

the stationary-phase point λ_s is given by

$$\Theta(\lambda_s) = -(2m\pi \mp \theta) . \tag{3.11}$$

Figure 16 shows the deflection function $\Theta_N(\lambda)$ of $S^0_{l_f,l_f}$ and $\Theta(\lambda)$, which includes also the Coulomb deflection function. There is *no* approximation of Eqs. (3.6) and (3.7) made in this figure, which indicates that only the $I_0^{(+)}(\theta)$ and $I_0^{(+)}(\pi-\theta)$ terms will contribute, i.e.,

$$F^M_L(\theta) \propto [I_0^{(+)}(\theta) + e^{iM\pi} I_0^{(+)}(\pi-\theta)] . \tag{3.12}$$

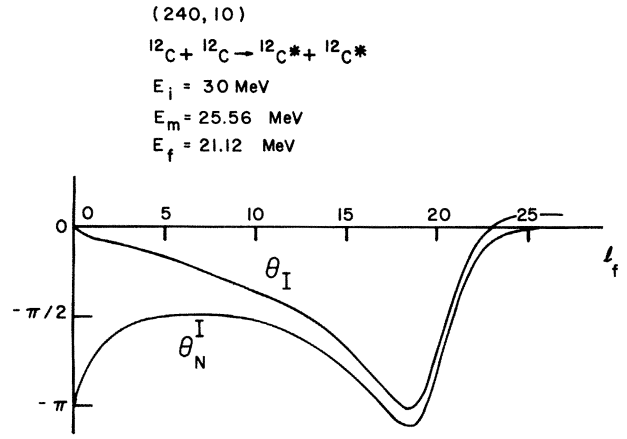

FIG. 16. The deflection function of $S^0_{l_f,l_f}$ is shown in this figure for a demonstration of the refractive effect in the scattering mechanism (see Ref. 9).

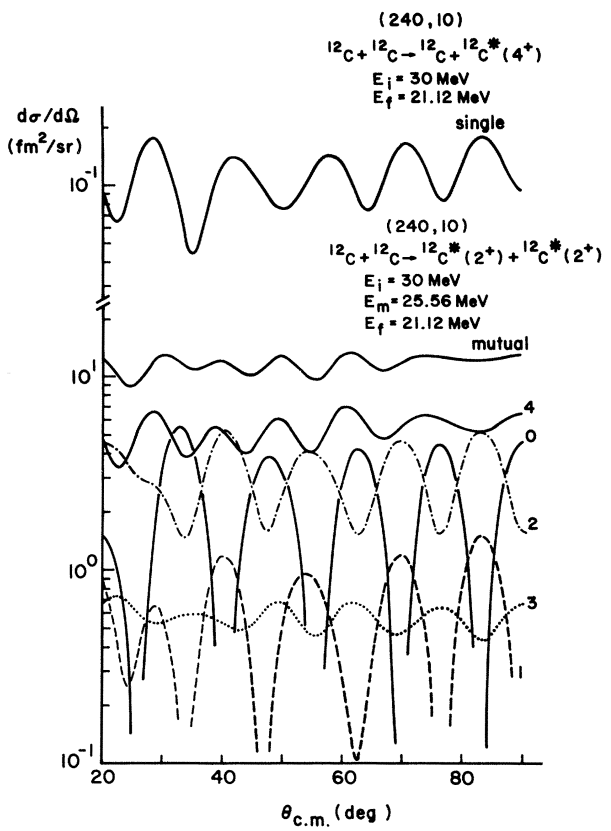

FIG. 17. Angular distributions of single, mutual, and double excitations are shown for comparison at weak absorption (W_0=10 MeV, V_0=240 MeV) (see the caption of Fig. 8 for detail).

Note that $I_0^+(\theta)$ and $I_0^+(\pi-\theta)$ are smooth functions of angle [Eq. (3.9)], with a refractive feature. However, the interference of $I_0^+(\theta)$ and $I_0^+(\pi-\theta)$ (identical ions) gives rise to oscillatory structure in the angular distribution. Figure 17 shows angular distribution of different L com-

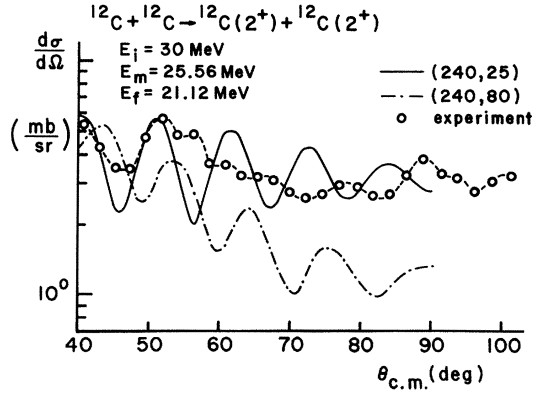

FIG. 18. Comparison of the cross section of the experimental mutual excitation data with that of our calculations with different imaginary strengths. In this qualitative study, we make no attempt to fit the data. Comparison of the slope of the calculated cross section to that of the experimental data indicates that the reaction mechanism in the mutual excitation of the $^{12}C + ^{12}C$ system is a refractive process. The relative strength of the imaginary potential reasonably agrees with that obtained in Ref. 14.

ponents, and one notes the following features:

(1) The $L=0$, 2, and 4 components contribute almost equally in magnitude. The $L=0$ component of the angular distribution has very deep minima seen in Eq. (3.12), but the minima of the $L=2$ and 4 angular distributions are filled in by the incoherent sum over M values.

(2) The $L=1$ and 3 components are not important (see Fig. 12 for comparison).

(3) The total angular distribution of the mutual excitation is now featureless and possesses very little oscillatory structure in comparison with those of the single and the two-phonon excitations (upper part of Fig. 16).

Finally, we compare the angular distribution given by our present calculation with the experimental mutual excitation data in Fig. 18. One notes that the refractive effect is very important as indicated by the data.[3] This refraction is due to a smaller imaginary potential being needed to fit the slope of the angular distribution. In this comparison, one also notes that our angular distribution does not follow the oscillatory structure of the data, since our optical potential is chosen only to study the general properties of second-order processes. Thus the comparison is a qualitative one, and to fit the data one should adjust the optical potential.[14] (See Ref. 9 for the choice of the optical potential parameters used in the present study.)

IV. CONCLUSION

We have studied the properties of the radial integral for second-order inelastic heavy-ion scattering, with the scattering mechanism divided into direct one-step (DOS) and two-step (TS) processes. Our conclusions are that:

(1) In the strong absorption limit, DOS and TS processes interfere destructively for angular momenta near to the grazing angular momentum. Using semiclassical theory we analyze carefully the origin of this interference, which causes the angular distribution for the second-order process to be flatter than that of the diffractive single excitations (see Fig. 9). The Austern-Blair theory provides us with a useful parametrization to understand the reaction process.

(2) For weak to moderate absorption, one observes that $B^{\rm DOS}_{l_f l_i}$ is not sensitive to the strength of the absorption potential (Sec. III A). The radial integral $B^{\rm TS}_{l_f l l_i}$ increases dramatically with decreasing imaginary potential strength. At $W_0/V_0 \cong 0.15 \sim 0.3$, the angular distribution remains diffractive in nature. The mutual excitation angular distribution shows, however, a destructive interference between $B^{\rm DOS}$ and $B^{\rm TS}$ processes at the grazing angle, and thus has a smaller slope.

(3) As the imaginary strength decreases further, $W_0/V_0 \leq 0.1$, we observe that the internal component, $B^{\rm TSI}$, of $B^{\rm TS}$ dominates the scattering process, and refraction becomes the major scattering mechanism. The angular distribution is then flat and featureless. From the qualitative comparison of our study with the experimental angular distribution of

$$^{12}\mathrm{C}+{}^{12}\mathrm{C}\rightarrow{}^{12}\mathrm{C}^{*}(2^{+})$$

at 30 MeV we find that $W_0/V_0 \simeq 0.1$ is appropriate for the slope of the angular distribution. To obtain a quantitative fit, one should fit the elastic scattering to obtain a mean-field potential and then calculate the mutual excitation cross section via a coupled-channel or DWBA calculation. At energy $E_{\rm c.m.} \cong 30$ MeV of the $^{12}\mathrm{C}+{}^{12}\mathrm{C}$ system, intermediate structure is still believed to be important,[14] and so the detailed angular distribution may not be easily fitted by the mean field alone.

ACKNOWLEDGMENTS

One of the authors (S.Y.L.) acknowledges many helpful discussions with Prof. P. Paul, Prof. R.L. McGrath, and Prof. D. B. Fossan of the Nuclear Structure Group at Stony Brook. We thank Prof. G. E. Brown for his encouragement of the work. We are grateful for Dr. David Dean in reading carefully through the paper. This work has been supported in part by USDOE Grant No. DEAC02-76-ER13001.

APPENDIX A: DERIVATION OF THE SECOND-ORDER SCATTERING AMPLITUDES

The Taylor-series expansion of the heavy-ion mean-field optical potential due to a small amplitude oscillation of the nuclear surface is given by

$$V(r,R_{01}+R_{02}+\Delta R_1+\Delta R_2)=V(r,R_{01}+R_{02})+\Delta V\ , \tag{A1}$$

where

$$\Delta V=\Delta R_1\frac{\partial V}{\partial R_{01}}+\Delta R_2\frac{\partial V}{\partial R_{02}}+\frac{1}{2}\left[(\Delta R_1)^2\frac{\partial^2 V}{\partial R_{01}^2}+2\Delta R_1\Delta R_2\frac{\partial^2 V}{\partial R_{01}\partial R_{02}}+(\Delta R_2)^2\frac{\partial^2 V}{\partial R_{02}^2}\right]+\cdots$$
$$=\sum_{n=1}^{\infty}\sum_{m=0}^{n}\frac{1}{m!(n-m)!}(\Delta R_1)^{n-m}(\Delta R_2)^m\frac{\partial^n V}{\partial R_{01}^{n-m}\partial R_{02}^m}\ , \tag{A2}$$

and $\Delta R_1, \Delta R_2$ are the changes in the nuclear radii of the heavy ions,

$$\Delta R_1=R_{01}\sum\beta^{(1)}_{\lambda\mu}Y^{*}_{\lambda\mu}(\hat{r})\ ,$$
$$\Delta R_2=R_{02}\sum\beta^{(2)}_{\lambda\mu}Y^{*}_{\lambda\mu}(\hat{r})\ . \tag{A3}$$

Upon quantization of the normal modes of the nuclear surface oscillation (or rotation),

$$\beta_{\lambda\mu}=\frac{1}{\sqrt{2B_\lambda\omega_\lambda}}[a^{+}_{\lambda\mu}+(-)^{\mu}a_{\lambda,-\mu}]\ ,$$

where $a^{+}_{\lambda\mu}$ and $a_{\lambda\mu}$ are the phonon creation and annihilation operators, respectively. Thus, ΔV in Eq. (A2) will give rise to collective excitation of these surface modes.

The inelastic transition amplitude is given by

$$T_{fi}=\langle\Phi_f\Psi_f^{(-)}\,|\,\Delta V+\Delta V G\Delta V\,|\,\Phi_i\Psi_i^{(+)}\rangle\ , \tag{A4}$$

where Φ_i and Φ_f are the intrinsic nuclear wave functions for the initial and final channels, and $\psi_f^{(-)}$ and $\psi_i^{(+)}$ are the regular distorted wave functions with the unperturbed mean field $V_0=V(r,R_0)$ satisfying the outgoing and incoming boundary condition, respectively. G is the full Green function; i.e.,

$$G=(E^+-H_I-K-V_0-\Delta V)^{-1}\ ,$$

with $E^+=E+i\epsilon$ and H_I and K being the intrinsic Hamiltonian of the nuclei and the relative kinetic energy operator; e.g., $H_I\Phi_i=\epsilon_i\Phi_i$, etc. Expanding G in the powers series of ΔV, we then obtain

$$G=G_0+G_0\Delta V G_0+\cdots\ , \tag{A5}$$

with

$$G_0=(E^+-H_I-K-V_0)^{-1}\ . \tag{A6}$$

Let us define the transition operator τ as

$$\begin{aligned}\tau&\equiv\Delta V+\Delta V G\Delta V\\&=\Delta V+\Delta G_0\Delta V+\Delta V G_0\Delta V G_0\Delta V+\cdots\\&=\sum_n\sum_i\tau_{ni}\ ,\end{aligned} \tag{A7}$$

where τ_{ni} will give rise to transition of the order $(\Delta R_1)^{n-i}(\Delta R_2)^i$, i.e., τ_{ni} is an operator for an nth order process:

$$\tau_{10}=\Delta R_1\frac{\partial V}{\partial R_{01}}\ , \tag{A8a}$$

$$\tau_{20}=\Delta R_2\frac{\partial V}{\partial R_{02}}\ , \tag{A8b}$$

$$\tau_{20}=\tfrac{1}{2}(\Delta R_1)^2\frac{\partial^2 V}{\partial R_{01}^2}+\Delta R_1\frac{\partial V}{\partial R_{01}}G_0\Delta R_1\frac{\partial V}{\partial R_{01}}\ , \tag{A8c}$$

$$\tau_{21}=\Delta R_1\Delta R_2\frac{\partial^2 V}{\partial R_{01}\partial R_{02}}+\Delta R_1\frac{\partial V}{\partial R_{01}}G_0\Delta R_2\frac{\partial V}{\partial R_{02}}+\Delta R_2\frac{\partial V}{\partial R_{02}}G_0\Delta R_1\frac{\partial V}{\partial R_{01}}\ , \tag{A8d}$$

$$\tau_{22}=\tfrac{1}{2}(\Delta R_2)^2\frac{\partial^2 V}{\partial R_{02}^2}+\Delta R_2\frac{\partial V}{\partial R_{02}}G_0(\Delta R_2)\frac{\partial V}{\partial R_{02}}\ , \tag{A8e}$$

$\vdots$

The intrinsic excitation of the nucleus is due to the β operators in the ΔR of Eq. (A3). The matrix element for the intrinsic excitation is given by

$$\langle L_j,M_j\,|\,(\Delta R_j)^i\,|\,00\rangle\equiv c_j^i(L_j)Y^*_{L_jM_j}(\hat r)\ , \tag{A9}$$

where the jth nucleus is excited from the ground state $|\,00\rangle$ to the ith order phonon state with angular momentum L_jM_j. $Y^*_{L_jM_j}(\hat r)$ is the angular momentum transfer spherical harmonic to acting on the relative DW function of two nuclei. A few examples are given as follows:

$$c_j^0(0)=\sqrt{4\pi}\ , \tag{A10a}$$

$$c_j^1(L)=\frac{1}{\sqrt{\hat L}}\langle L\,||\beta_L||\,0\rangle R_{0j}=\frac{1}{\sqrt{\hat L}}\delta_L^{(j)}\ , \tag{A10b}$$

$$c_j^2(L)=\frac{1}{\sqrt{4\pi\hat L}}\delta_{\lambda_1}^{(j)}\delta_{\lambda_2}^{(j)}\langle\lambda_1 0\lambda_2 0\,|\,L\,0\rangle+(\lambda_1\leftrightarrow\lambda_2;\ \text{if}\ \lambda_1\neq\lambda_2)\ , \tag{A10c}$$

$\vdots$

where $\hat L=2L+1$, the deformation length is defined in Eq. (A10b), and two-phonon states are used in Eq. (A10c). The double- and mutual-excitation transition amplitude is then given as the following.

A. Double excitation

If the particle 1 is excited from the ground state to the two-phonon state

$$|\,LM\rangle=\frac{1}{\sqrt{2}}[a^+_{\lambda_1}\times a^+_{\lambda_2}]^{LM}\,|\,0\rangle\ ,$$

the transition operator τ_{20} in Eq. (A8c) is composed of two terms, direct one-step (DOS) and two-step (TS) processes, and the transition amplitude becomes

$$\begin{aligned}T^D_{00\to LM}&=\delta^{(1)}_{\lambda_1}\delta^{(1)}_{\lambda_2}\sum_{l_fl_i}i^{l_i-l_f}e^{i(\sigma_{l_f}+\sigma_{l_i})}\sqrt{\hat l_f}\langle l_f-M,LM\,|\,l_i0\rangle Y_{l_f-M}(\theta,0)\langle\lambda,0,\lambda_20\,|\,L\,0\rangle\\&\quad\times\sum_{L'}\langle l_f0L'0\,|\,l_i0\rangle\left[\tfrac{1}{2}\delta_{LL'}B^{\rm DOS}_{l_fl_i}+\sum_l\hat l\sqrt{\hat L\hat L'}\begin{Bmatrix}l_f&l_i&L\\\lambda_2&\lambda_1&l\end{Bmatrix}\begin{Bmatrix}l_f&l_i&L'\\\lambda_2&\lambda_1&l\end{Bmatrix}B^{\rm TS}_{l_f,l_1,l_i}\right]+(\lambda_1\leftrightarrow\lambda_2\ \text{if}\ \lambda_1\neq\lambda_2)\\&=\sqrt{\hat L}\,\delta^{(1)}_{\lambda_1}\delta^{(1)}_{\lambda_2}\sum_{l_fl_i}i^{l_i-l_f}e^{i(\sigma_{l_f}+\sigma_{l_i})}\sqrt{\hat l_f}\langle l_f-M,L,M\,|\,l_i0\rangle Y_{l_f-M}(\theta,0)\\&\quad\times\sum_l\sqrt{\hat l}\langle l_f0\lambda,0\,|\,l0\rangle\langle l0\lambda_20\,|\,l_i0\rangle\begin{Bmatrix}l_f&l_i&L\\\lambda_2&\lambda_1&l\end{Bmatrix}(\tfrac{1}{2}B^{\rm DOS}_{l_fl_i}+B^{\rm TS}_{l_f,l,l_i})+(\lambda_1\leftrightarrow\lambda_2;\ \text{if}\ \lambda_1\neq\lambda_2)\ .\end{aligned} \tag{A11}$$

The first identity of Eq. (A11) has the advantage that its appearance is similar to that of the single excitation. The second identity of Eq. (A10) shows, however, the explicit interference between the DOS and TS radial integrals, which are given by

$$B^{\mathrm{DOS}}_{l_f,l_i}=\frac{\sqrt{4\pi}}{k_f k_i}\int dr f_{l_f}(k_f,r)V^{(2)}_T f_{l_i}(k_i,r)dr\ , \tag{A12a}$$

$$B^{\mathrm{TS}}_{l_f,l,l_i}=\frac{\sqrt{4\pi}}{k_f k_i}\int\int dr_1 dr_2 f_{l_f}(k_f,r_1)V^{(1)}_T(r_1)\frac{-2\mu}{k}f_l(k,r_<)h^{(+)}_l(k,r_>)V^{(1)}_T f_{l_i}(k_i,r)\ . \tag{A12b}$$

B. Mutual excitation

Mutual excitation in heavy ion collision corresponds to particle 1 and particle 2 being excited to states $|\lambda_1\mu_1\rangle$ and $|\lambda_2\mu_2\rangle$, respectively. The transition operator is τ_{21}, which consists of DOS and TS processes. The transition operator is given by

$$\begin{aligned}T^M_{00\to\lambda_1\mu_1\lambda_2\mu_2}&=\delta^{(1)}_{\lambda_1}\delta^{(2)}_{\lambda_2}\sum_{l_f l_i} i^{l_i-l_f}e^{i(\sigma_{l_i}+\sigma_{l_f})}\sqrt{\hat{l}_f}\\
&\quad\times\sum_{LL'}\langle l_f-M,L,M\,|\,l_2 0\rangle\langle\lambda_1\mu_1,\lambda_2\mu_2\,|\,LM\rangle\langle l_f 0L'0\,|\,l_i 0\rangle\langle\lambda_1 0\lambda_2 0\,|\,L'0\rangle Y_{l_f-M}(\theta,0)\\
&\quad\times\left[\tfrac{1}{2}\delta_{LL'}B^{\mathrm{DOS}}_{l_f,l_i}+\sum_l \hat{l}\sqrt{\hat{L}\hat{L}'}\begin{Bmatrix}l_f & l_i & L\\ \lambda_2 & \lambda_1 & l\end{Bmatrix}\begin{Bmatrix}l_f & l_i & L'\\ \lambda_2 & \lambda_1 & l\end{Bmatrix}B^{\mathrm{TS}}_{l_f,l,l_i}\right]+(\lambda_1\mu_1\leftrightarrow\lambda_2\mu_2)\\
&=\delta^{(1)}_{\lambda}\delta^{(2)}_{\lambda}\sum_{l_f l_i} i^{l_i-l_f}e^{i(\sigma_{l_i}+\sigma_{l_f})}\sqrt{\hat{l}_f}\\
&\quad\times\sum_L\sqrt{\hat{L}}\langle l_f-M,LM\,|\,l_i 0\rangle\langle\lambda_1\mu_1\lambda_2\mu_2\,|\,LM\rangle Y_{l_f-M}(\theta,0)\\
&\quad\times\sum_l\sqrt{\hat{l}}\langle l_f 0\lambda_1 0\,|\,l0\rangle\langle l0,\lambda_2 0\,|\,l_i 0\rangle\\
&\quad\times\begin{Bmatrix}l_f & l_i & L\\ \lambda_2 & \lambda_1 & l\end{Bmatrix}(\tfrac{1}{2}B^{\mathrm{DOS}}_{l_f l_i}+B^{\mathrm{TS}}_{l_f,l,l_i})+(\lambda_1\mu_1\leftrightarrow\lambda_2\mu_2)\ ,\end{aligned} \tag{A13}$$

where the radial integrals B^{DOS} and B^{TS} are the same as that of Eq. (A11) due to the fact that V_0 is a symmetry with the exchange of R_{10} and R_{20}. The difference between Eqs. (A11) and (A13) is that Eq. (A13) has a coherent sum of transfer angular momentum.

Defining the inelastic S matrix $S^L_{l_f l_i}$ as

$$\begin{aligned}S^L_{l_f,l_i}&=2i\sqrt{k_i}k_f\delta_{\lambda_1}\delta_{\lambda_2}\frac{\mu}{4\pi^{3/2}}\sum_{L'}\langle l_f 0,L'\,|\,l_1 0\rangle\langle\lambda_1 0,\lambda_2 0\,|\,L'0\rangle i^{l_i-l_f}\\
&\quad\times\left[\tfrac{1}{2}\delta_{LL'}B^{\mathrm{DOS}}_{l_f,l_i}+\sum_l\hat{l}\sqrt{\hat{L}\hat{L}'}\begin{Bmatrix}l_f & l_i & L\\ \lambda_2 & \lambda_1 & l\end{Bmatrix}\begin{Bmatrix}l_f & l_i & L'\\ \lambda_2 & \lambda_1 & l\end{Bmatrix}B^{\mathrm{TS}}_{l_f,l,l_i}\right]\\
&\quad+\begin{cases}(\lambda_1\leftrightarrow\lambda_2)\ \text{mutual}\\ (\lambda_1\leftrightarrow\lambda_2\ \text{if}\ \lambda_1\neq\lambda_2)\ \text{double}\ ,\end{cases}\end{aligned} \tag{A14}$$

the scattering amplitude becomes

$$\begin{aligned}F^D_{LM}(\theta)&=\frac{\mu}{2\pi}T^D_{00\to LM}\\
&=\frac{1}{2i\sqrt{k_i k_f}}\sum_{l_i l_f}\sqrt{4\pi\hat{l}_f}e^{i(\sigma_{l_i}+\sigma_{l_f})}\langle l_f-M,LM\,|\,l_i 0\rangle S^L_{l_f l_i}Y_{l_f-M}(\theta,0)\ ,\end{aligned} \tag{A15}$$

where Eq. (A15) resembles closely with the elastic scattering amplitude. The corresponding mutual excitation scattering amplitude is $F^M_{00\to\lambda_1\mu_1\lambda_2\mu_2}(\theta,0)$. The differential cross sections for double and mutual excitation are given, respectively, by

$$\frac{d\sigma^D}{d\Omega}=\frac{k_f}{k_i}\sum_M |F^D_{LM}(\theta)|^2 , \tag{A16a}$$

$$\frac{d\sigma^M}{d\Omega}=\frac{k_f}{k_i}\sum_{\mu_1\mu_2} |F^M_{00\to\lambda,\mu,\lambda_2,\mu_2}|^2 . \tag{A16b}$$

APPENDIX B: ELASTIC BARRIER WAVE S MATRIX AND ITS DERIVATIVE FOR SMALL ANGULAR MOMENTUM

The elastic barrier wave S matrix, η_B, is defined as

$$\eta_B=\frac{e^{2i\delta_1(l)}}{N(l)} , \tag{B1}$$

with $N(l)=N(S_{21}(l)/\pi)$,

$$\delta_1(l)=\int_{r_1}^{\infty}\sqrt{\chi(r)}dr-\int_{r_c}^{\infty}\sqrt{\chi_c(r)}dr , \tag{B2}$$

where

$$\chi(r)=2\mu(E-V_c-V_l-V)$$

and

$$\chi_c=2\mu(E-V_c-V_l) .$$

For small angular momentum and light ions ($A_1,A_2\le 30$ u), V_l and V_c are almost constant compared to V at r near the outer turning point. With a small change $R_0\to R_0+\Delta R_0$, the turning point r_1 will also change slightly to $r_1\to r_1+\Delta R_1$. The change in the action integral (B2) becomes

$$\Delta\delta_1=\int_{r_1+\Delta R_1}^{\hat{r}}\sqrt{\chi}dr\simeq-\sqrt{\chi_1(r_1)}\Delta R_1 \simeq-\sqrt{\chi(r_1)}\Delta R_0 . \tag{B3}$$

Thus,

$$\frac{\partial\eta_\beta}{\partial R_0}\simeq 2i\frac{\partial\delta_1}{\partial R_0}\eta_\beta=-2i\sqrt{\chi(r_1)}\eta_\beta=-2ik_c\eta_\beta , \tag{B4}$$

$$\frac{\partial^n\eta}{\partial R_0^n}\simeq(-2ik_c)^n\eta_\beta , \tag{B5}$$

where k_c is the local wave number at the barrier.

APPENDIX C: COLLECTIVE EFFECT OF OVERLAPPING RESONANCES

In this Appendix, we show that overlapping resonances work coherently to give rise to a refractive effect in the scattering process. Let us consider a picket fence model, where the Regge poles and zeros are equally spaced locating at $mD+i\gamma_p/2$ and $mD-i\gamma_z/2$, respectively, with $m=-M,-M+1,\ldots,M-1,M$. The S matrix for angular momentum $-MD\le l\le MD$ can be expressed as

$$S_l=e^{2i\phi}\prod_{m=-M}^{M}\frac{l-mD+i\frac{\gamma_z}{2}}{l-mD-i\frac{\gamma_p}{2}} =e^{2i\phi}\prod_{m=-M}^{M}\left[\frac{\frac{m-N_z}{D}}{\frac{m-N_p}{D}}\right] , \tag{C1}$$

where ϕ represents the background phase and $N_z=l+i\gamma_z/2$, $N_p=l-\gamma_p/2$. Using the property of the gamma function, Eq. (1) can be expressed as

$$S_l=e^{2i\phi}\frac{\Gamma\left[M+1-\frac{N_z}{D}\right]\Gamma\left[M+1+\frac{N_z}{D}\right]}{\Gamma\left[M+1-\frac{N_p}{D}\right]\Gamma\left[M+1+\frac{N_p}{D}\right]}\frac{\sin\frac{\pi N_z}{D}}{\sin\frac{\pi N_p}{D}} \simeq S_0\frac{\sin\left[\frac{\pi l}{D}+i\frac{\pi\gamma_z}{2D}\right]}{\sin\left[\frac{\pi l}{D}-i\frac{\pi\gamma_p}{2D}\right]} . \tag{C2}$$

For $M\gg 1$, the gamma functions are slowly varying the function of l, and can be lumped into a background S matrix S_0. Defining

$$t_z=\tanh\frac{\pi\gamma_z}{2D} , \qquad t_p=\tanh\frac{\pi\gamma_p}{2D} , \tag{C3}$$

we obtain

$$S_l=S_0\frac{\cosh\frac{\pi\gamma_z}{2D}}{\cosh\frac{\pi\gamma_p}{2D}}\left[\frac{t_p-t_z}{2t_p}+\frac{t_p+t_z}{2t_p}\frac{\tan\frac{\pi l}{D}+it_p}{\tan\frac{\pi l}{D}-it_p}\right] =\frac{S_0}{\sinh\frac{\pi\gamma_p}{D}}\left[\sinh\frac{\pi(\gamma_p-\gamma_z)}{D}-\sinh\frac{\pi(\gamma_p+\gamma_z)}{D}e^{2i\delta_l}\right] , \tag{C4}$$

with

$$\delta_l=-\tan^{-1}\left[\frac{\tan\frac{\pi l}{D}}{t_p}\right] . \tag{C5}$$

One observes that: (1) when $\gamma_p=\gamma_z>D$, i.e., with no absorption and with overlapping resonances, S_l is unitary with phase shift δ_l; (2) when $\gamma_p>\gamma_z>0$ and $\gamma_p>D$ (moderate absorption), the second term in the bracket of Eq. (C4) is much more important; S_l still carries an important signature of these resonances, i.e., $\delta_l=-\pi l/D$; (3) when $\gamma_p>D,\gamma_z<0$, i.e., the absorption is so important that the Regge zero crosses the real angular momentum

axis, the first term in Eq. (C5) becomes more important than the second term. Then all the information of these resonances will recede to the background strong absorption limit and the magnitude of the S matrix becomes

$$|S_l| \sim |S_0| e^{-|\gamma_p - \gamma_z|/2D} .$$

$|S_l|$ can be very small, but it is impossible to have $|S_l| \to 0$ in the present model. One notes, however, that the *manifestation of strong absorption comes also from the slow dependence of the phase shift on the angular momentum.*

From the above discussion, we therefore conclude that the effect of overlapping undamped resonances is to give rise to a phase shift $\delta_l \cong \pi l/D$ or equivalently to a deflection function

$$\Theta_l \cong \frac{d}{dl}(2\delta_l) = -\frac{2\pi}{D}$$

(refractive effect).

[1]T. M. Cormier *et al.*, Phys. Rev. Lett. 38, 940 (1977).

[2]T. M. Cormier *et al.*, Phys. Rev. Lett. 40, 924 (1978).

[3]R. Wieland, Ph.D. dissertation, Yale University, 1973 (unpublished).

[4]R. Wieland *et al.*, Phys. Rev. C 8, 37 (1973).

[5]R. McGrath *et al.* (private communication); and (unpublished).

[6]N. Austern and J. S. Blair, Ann. Phys. (N.Y.) 33, 15 (1965); F. J. W. Hahne, Nucl. Phys. A104, 545 (1967); A106, 660 (1968).

[7]R. M. Drisko, G. R. Satchler, and R. H. Bassel, Phys. Lett. 5, 347 (1963); R. H. Bassel, G. R. Satchler, and R. M. Drisko, Nucl. Phys. 89, 419 (1966).

[8]R. H. Lemmer, A. de Shalit, and N. S. Wall, Phys. Rev. 124, 1155 (1961); B. Buck, *ibid.* 127, 940 (1962); N. Austern, R. M. Drisko, E. Rost, and G. R. Satchler, *ibid.* 128, 733 (1962).

[9]Y. H. Chu and S. Y. Lee, Nucl. Phys. A369, 514 (1981).

[10]D. M. Brink and N. Takigawa, Nucl. Phys. A279, 159 (1977); S. Y. Lee, N. Takigawa, and C. Marty, *ibid.* A308, 161 (1978); N. Takigawa and S. Y. Lee, *ibid.* A292, 159 (1977).

[11]S. Y. Lee and N. Takigawa, Nucl. Phys. A308, 189 (1978).

[12]N. Austern, Ann. Phys. (N.Y.) 15, 299 (1961); *Direct Nuclear Reaction Theories* (Wiley, New York, 1970).

[13]See for example, D. M. Brink, in *Nuclear Physics with Heavy Ions and Mesons,* edited by R. Balian, M. Rho, and G. Ripka (North-Holland, Amsterdam, 1977), Vol. 1.

[14]S. Y. Lee, H. W. Wilschut, and R. Ledoux, Phys. Rev. C 25, 2844 (1982).